Journal of
Marine Science and Engineering

MDPI

Article

Research on the Effect of Burial Depth on The Bearing Characteristics of Three Helical Piles Jacket Foundation for Offshore Wind Turbines

Changyang Ouyang [1], Jianhua Luo [2], Tingyuan Wang [2] and Puyang Zhang [2,*]

[1] Wind Power Research and Development Division, Engineering Research Center, CRRC Zhuzhou Electric Co., Ltd., Zhuzhou 412000, China
[2] State Key Laboratory of Hydraulic Engineering Simulation and Safety, Tianjin University, Tianjin 300354, China
* Correspondence: zpy@tju.edu.cn

Abstract: With global offshore wind power gradually moving to deep and distant waters, there is a clear trend towards larger-scale units, posing significant challenges for future offshore wind power foundations. In this paper, a helical pile jacket foundation type is proposed by combining the advantages of the current jacket foundation, which is suitable for deep and distant seas and offers high stiffness, with the excellent bearing performance of helical pile foundations. The influence of buried depth on the bearing characteristics of this foundation type is discussed through a physical model test. The results obtained from the study reveal the distinct bearing characteristics and damage modes exhibited by the foundation under deep and shallow burial conditions. These findings clearly indicate that the overall bearing characteristics and damage modes are superior in deep burial conditions compared to shallow burial conditions. Furthermore, it is observed that the damage and displacement of the foundation are more concentrated in localized areas when subjected to shallow burial.

Keywords: offshore wind power; deep offshore; helical pile; load bearing characteristics

Citation: Ouyang, C.; Luo, J.; Wang, T.; Zhang, P. Research on the Effect of Burial Depth on The Bearing Characteristics of Three Helical Piles Jacket Foundation for Offshore Wind Turbines. *J. Mar. Sci. Eng.* **2023**, *11*, 1703. https://doi.org/10.3390/jmse11091703

Academic Editor: Erkan Oterkus

Received: 6 July 2023
Revised: 17 August 2023
Accepted: 24 August 2023
Published: 29 August 2023

1. Introduction

The vigorous advancement of offshore wind power is not solely a pivotal lever to ensure energy security and propel economic growth for various nations, but also a critical pathway for global collaboration in addressing the climate crisis and building a shared destiny for all humanity. In recent years, China's offshore wind power development has accelerated significantly, installing world-leading capacity. However, due to the ecological protection of the environment, traffic channel occupation, and other factors, offshore wind power resources are increasingly tight. The deep sea has more extensive sea resources and richer wind energy reserves and the development potential is greater; therefore, offshore wind power to deep sea and large units is an inevitable trend. However, high megawatts and the reliability of offshore wind turbine foundation requirements are more demanding; the disadvantages of traditional pile foundation with the harsh environment of the deep sea have gradually been highlighted. As such, the development of a new foundation type applicable to deep sea research is imperative.

Due to the existence of helical vanes, the area of interaction with soil in the process of compressive and pullout resistance is increased, which gives its axial bearing capacity a large increase, and also has a large bearing capacity advantage compared with conventional piles [1–3]. Furthermore, after its combination with the stiffness and low geological requirements of the conduit frame, this helical pile jacket foundation has a great bearing capacity advantage for large megawatt models under large bending moment and large shear load environment in deep and distant sea. It has great bearing capacity advantages and has certain advantages in construction efficiency and quality compared with traditional pile foundations in the field of deep-sea construction [4,5]. Therefore, the helical pile jacket foundation has great potential for offshore wind power projects in deep waters.

Related scholars have conducted studies on the bearing capacity of helical pile groups [6–11]. Their focus has primarily been on the efficiency of group piles, settlement ratio, and load transfer mechanism. In these studies, the selected research objects were typically group pile foundations with a bearing platform, consisting of numerous piles with small diameters and close spacing. However, there is a relative scarcity of research on the specific load characteristics of large megawatt-class units in the context of offshore wind power, which involve significant bending moments and horizontal forces. Except for one study [12], little attention has been given to these aspects. In addition, the study [12] focuses specifically on the pullout force, rather than the bending moment and horizontal force, which are crucial considerations for offshore wind power projects in deep-sea environments. At the same time, the burial depth has a decisive influence on the bearing capacity and bearing mode of the pile foundation. Considering the expensive construction cost and the harsh construction environment of the deep sea, it is necessary to conduct relevant research on the effect of burial depth on the bearing capacity and bearing mode of the triple helix pile jacket foundation, in order to create some guidelines for the actual project.

Considering the applicability of the helical pile conduit frame for offshore wind power and the scarcity of related research, this paper proposes a novel helical pile jacket foundation. It combines the advantages of the conduit frame, including higher structural stiffness, mature technology, and simplified operational procedures [13,14]. Moreover, it incorporates the excellent bearing performance of the helical pile foundation [4,15–22]. In order to investigate the bearing performance of the triple helical pile jacket foundation at varying burial depths, physical model tests were conducted as part of an exploratory study. The aim of these tests was to gain insights into how the foundation performs under different conditions. The research results can provide new ideas for the design of helical pile jacket foundation for offshore wind power in deep and distant waters and provide some theoretical reference and engineering guidance value for the selection of offshore wind power foundation in deep waters.

2. Experimental Design

2.1. Experimental Model Design

The physical model of the foundation structure is shown in Figure 1 below, and the dimensions of the physical model are shown in Figure 2. We used a model scale of 1:60, in which the diameter of the spreader bar is 18 mm, the diameter of the main bar is 32 mm, the thickness of both is 2 mm, the thickness of the pile body is 3 mm, and the thickness of the helical blade is 1 mm. The whole foundation structure consists of three parts: the conduit frame, the connecting frame, and the helical pile, in which the conduit frame mainly consists of these parts: the connecting frame is a triangular square steel tube frame at the top of the pile flange in Figure 1; the connecting frame itself is fixed to the conduit frame by bolts, and a screw is fixed on the pile body, while the pile body axis coincides with the screw axis, and the screw then passes through a hole on the frame located directly above the pile body axis. The screw then passes through a hole in the frame located directly above the axis of the pile, and is fixed to the frame by the nut on the screw, thus bearing the axial force of the pile body. The node connection details are shown in Figure 3. Figure 4 shows the number and spacing of different blades of the foundation to achieve the way, the helical blade is fixed on the connection sleeve, and the connection sleeve is connected to the pile body by screws.

Figure 1. Schematic diagram of the experimental model.

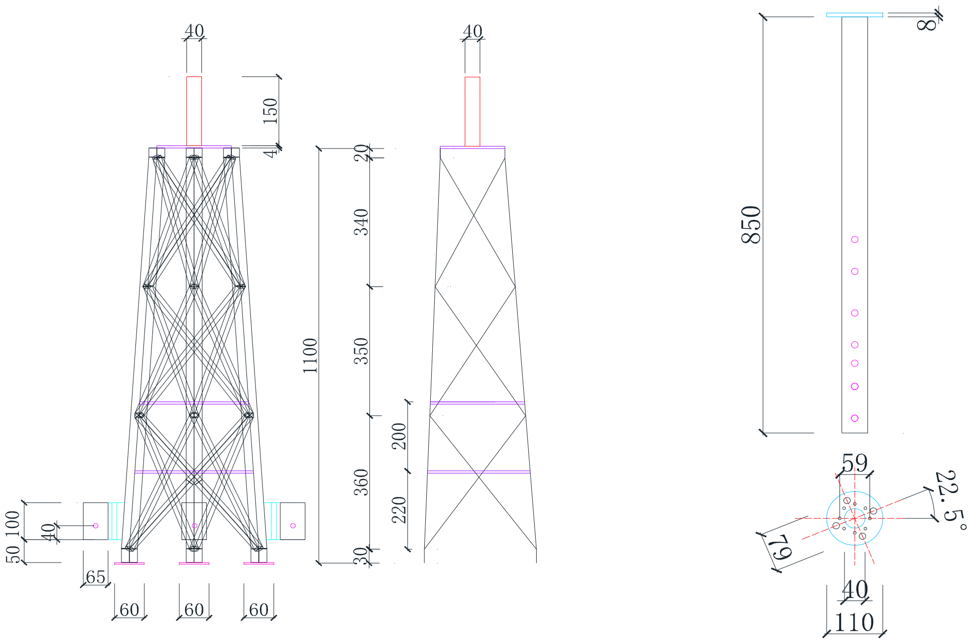

Figure 2. Schematic diagram of the foundation dimensions of the helical pile conduit frame.

Figure 3. Connection node details.

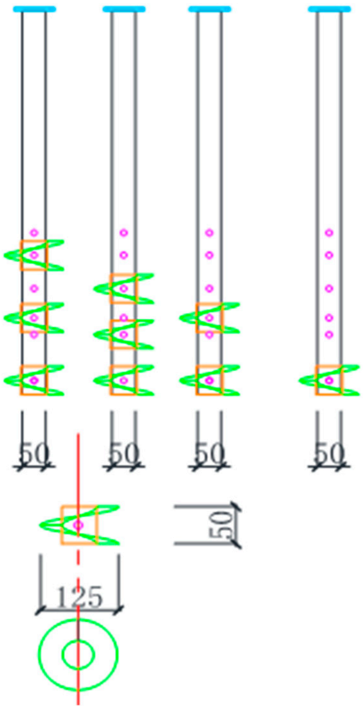

Figure 4. Helical pile different blade number, spacing to achieve the way.

2.2. Test Loading Devices

The loading device is a servo-electric cylinder for horizontal loading, the horizontal loading capacity of the electric cylinder is 1 T, and the maximum speed can be 62.5 mm/s. As shown in Figure 5, the electric cylinder can be driven by the filament rod and the front few to carry out the change of loading height. The displacement load curve is obtained by the loading device, in which the force is collected by the spoke type pull pressure sensor at the contact end of the electric cylinder. The loaded reaction force and displacement information is automatically captured by the control operating system of the electric cylinder record. The size of the soil tank used for the test is $2 \times 2 \times 1.5$, the depth of the soil tank is 1.5 m, where the depth of the soil layer is 1.2 m, the sand in the soil tank is Fujian standard sand, and its parameters are shown in Table 1.

Figure 5. Horizontal loading device.

Table 1. Principal parameters of the foundation.

Dr	k (cm/s)	φ (°)	Gs	c (kPa)	W (%)	e
0.45	0.0039	31.8	2.67	2.5	22.41	0.57

In Table 1, Dr is the relative density, k is the permeability coefficient, φ is the internal friction angle, Gs is the relative density, c is the internal cohesion, W is the water content, and e is the void ratio.

2.3. Test Sandy Soil

The soil used in the test is Fujian standard sand, and the parameters of the soil are shown in Table 1. For the soil test, loading will produce damage in the soil body, so a steel tube for each test needs to be used for turning soil loose. For the soil body remodeling, due to the soil body being relatively large, an auger is used for the remodeling of the soil body. The auger is shown in Figure 6 below. The specific process is to drill holes within a predetermined range of loosened soil. Initially, a hole is drilled to a depth of 1.2 m, followed by a second hole at the point where the two circles are tangential to each other. The new soil is then rotated into the previous hole and so on until all the soil within the remodeling area has been loosened.

2.4. Data Type and Sensors Used

The test collected data in four main areas: displacement load data, pile shaft force, foundation displacement, and soil pressure around the helical vane:

(1) Displacement load data

The displacement load data are measured by the loading device, which is a horizontally loaded electric cylinder, as shown in Figure 5 above. The force is collected by the spoke type pulling pressure sensor at the contact end of the electric cylinder, and the loaded reaction force and displacement information is automatically captured and recorded by the control operating system of the electric cylinder.

(2) Pile shaft force

As shown in Figure 7 below, the sensor used for axial force is a spoke type sensor, with a sensor range of ±500 kg, a tension sensor. The sensor and the pile top flange are fixed by bolts, and then the sensor is connected to the force transmission frame on the conduit frame through the screw and nut. The hole through the screw on the force transmission frame is much larger than the diameter of the screw. The axial force is applied to the sensor through the screw.

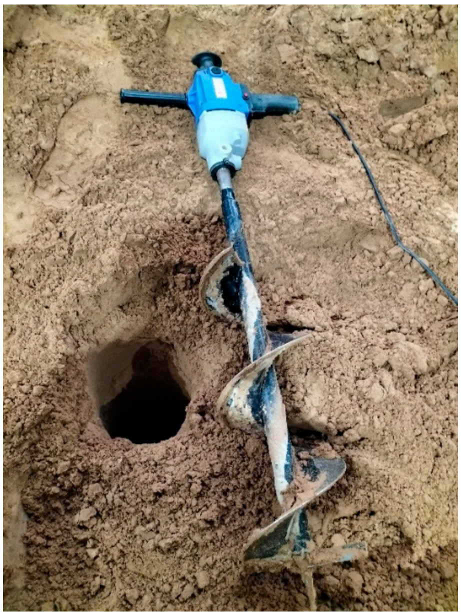

Figure 6. Soil remodeling equipment.

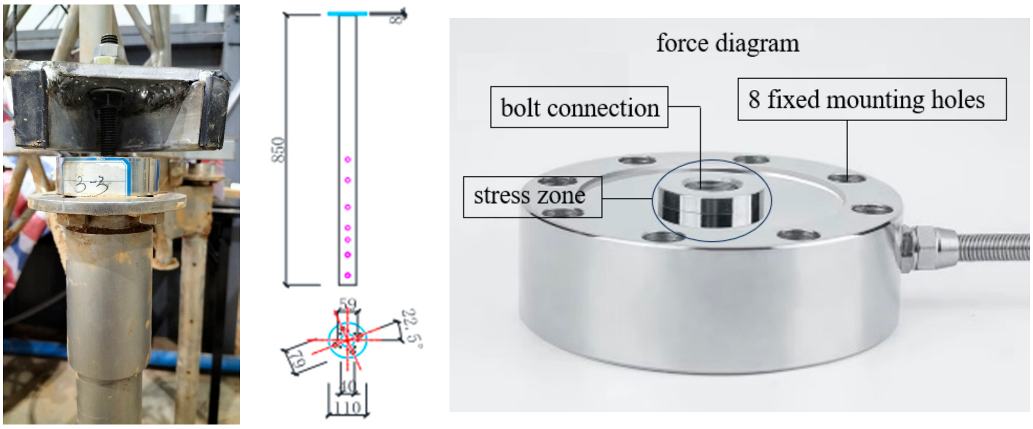

Figure 7. Schematic diagram of axial force sensor and its connection structure.

(3) Base displacement

The determination of the foundation displacement uses the pull-wire displacement meter. The displacement measurement range is 1 m and the accuracy is 0.0001 mm. Four items are measured in the displacement: horizontal displacement of tension pile a_1, vertical displacement of tensioned pile b_1, horizontal displacement of a pile under pressure a_2, and vertical displacement of a pile under pressure b_2. The sensors of a_1 and b_1 are connected to the top of the tensioned pile. The sensors of a_2 and b_2 are connected to the top of the pressurized pile. As the sensor connection end point moves with the structure during the horizontal loading of the foundation, as shown in Figure 8d, the connection point between the pull wire displacement gauge and the structure moves from point a to point b. Therefore, it is necessary to further process the data of the displacement sensor in order to get the actual displacement data. Since the distance of the sensor placement point from the measurement point for measuring the horizontal displacement is much larger than the vertical displacement of the measurement point, it is considered that the horizontal displacement of the measurement point is the actual change value shown by the sensor measurement. However, for the vertical displacement of the measurement point, there is a geometric relationship as shown in Figure 8a, and the following calculation formula can be obtained, where L1 is the initial length of the sensor pulling wire, L2 is the final length, L is the horizontal displacement value, and H is the actual axial displacement:

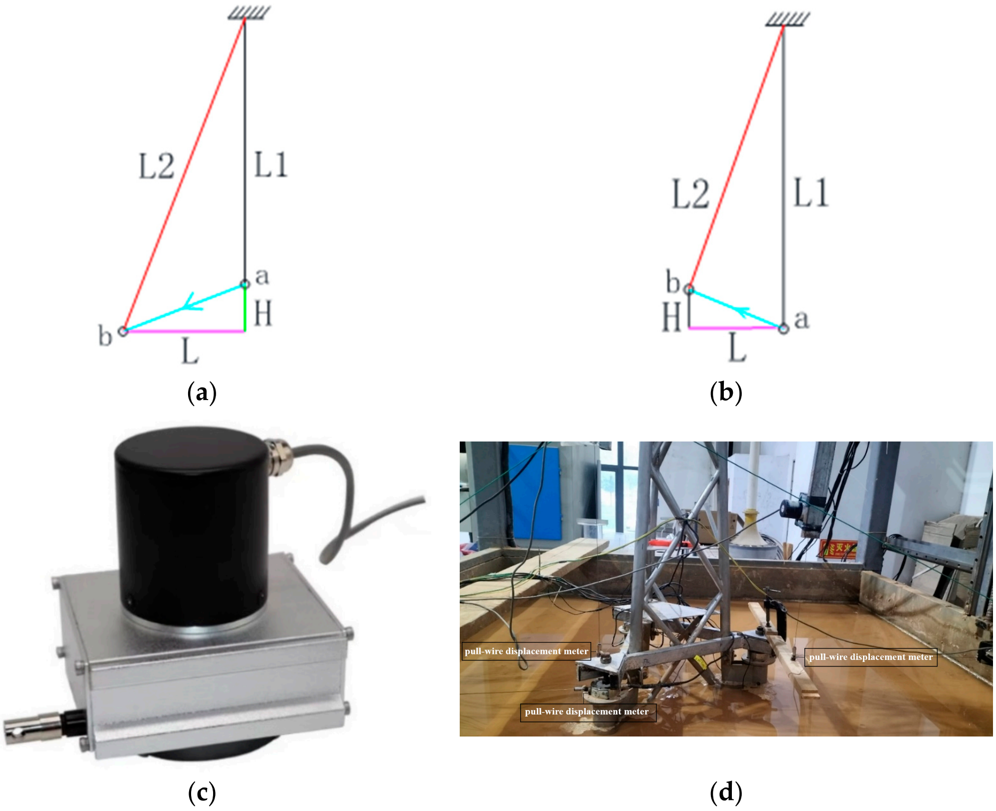

Figure 8. Displacement sensor and its arrangement. (**a**) Geometry of pile displacement under pressure; (**b**) Geometry of pile displacement under tension; (**c**) Pull-wire displacement meter; (**d**) Displacement sensor connection and arrangement.

Pressurized piles:

$$H = (L2^2 - L^2)^{0.5} - L1$$

Tensioned piles:

$$H = L1 - (L2^2 - L^2)^{0.5}$$

(4) Soil pressure around the spiral blade

In order to be able to reflect the working state of the helical blade, the vibration string type earth pressure sensor is glued on the blade with a waterproof adhesive. the range of the sensor is 50 kPa, as shown in the Figure 9, and the diameter of the sensor is 19 mm. The location of the measured earth pressure is the upper and lower blade of the tension pile, and the upper and lower blade of the pressure pile.

2.5. Test Procedure

The main process of the test is: (1) soil reshaping after each test (range 1.9 m × 1.9 m × 1.2 m), (2) digging holes at predetermined locations to predetermined burial depths, (3) lifting and placing the foundation by the yellow crane at the top right of the figure, then backfilling the soil evenly, (4) slowly releasing water into the soil box through the water pipe connected to the outlet pipe network at the bottom of the box until 5 cm above the soil surface, (5) the soil is left to stand for 24 h, (6) horizontal displacement is applied, (7) water is released through the outlet pipe at the bottom of the soil box.

Figure 9. Soil pressure sensor.

3. Comparison of Load-Bearing Performance of Three Helical Piles Jacket Foundation at Different Burial Depths

3.1. Bearing Capacity at Different Burial Depths

An exploratory study was conducted to investigate the bearing capacity of a three-pile guide frame foundation under shallow burial conditions at a depth of 4 times the diameter of the bottom blade (referred to as "D50") and under deep burial conditions at a depth of 6.5 times the diameter of the bottom blade (referred to as "D75"). The loading directions were divided into three scenarios: x, y, and my, as depicted in Figure 10. These were represented as d-x, d-y, and d-my, respectively: d-x denotes the compressive load on the L-pile and tensile load on the P-pile under lateral resistance, d-y indicates the compressive load on the Y-pile and tensile loads on both the P-pile and L-pile, and d-my represents the tensile load on the Y-pile, with compressive loads on the P-pile and L-pile.

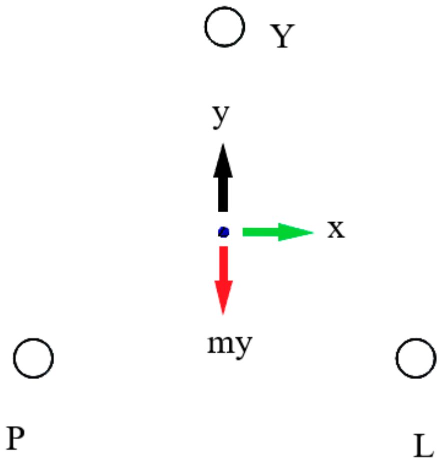

Figure 10. Schematic diagram of different loading directions of the foundation.

3.1.1. Compression Load on a Single Pile (d-y)

Figure 11 illustrates the bearing capacity of Y1L1 at different burial depths, highlighting the significance of burial depth in foundation strength. Specifically: (a) At a burial depth of 6.5 times the diameter of the bottom blade in the three-pile guide frame foundation, the bearing capacity is substantially greater than that at a burial depth of 4 times the blade diameter. The most notable disparity in bearing capacity is observed in the d-my loading scenario, where the bearing capacity at 6.5 times the blade diameter is nearly twice that at 4 times the blade diameter. (b) In terms of the relative bearing capacity for d-y and d-my loading scenarios, the relative sizes of the two loading directions at 6.5 times the blade diameter are superior to those at 4 times the blade diameter. The difference in bearing capacity between the single-pile side and the double-pile side is inherent to foundation strength. Furthermore, the tensile loading condition is the most unfavorable for pile foundations. The upper soil pressure on tensile piles is of paramount importance, and a decrease in burial depth, as observed in the graph, weakens the d-my scenario.

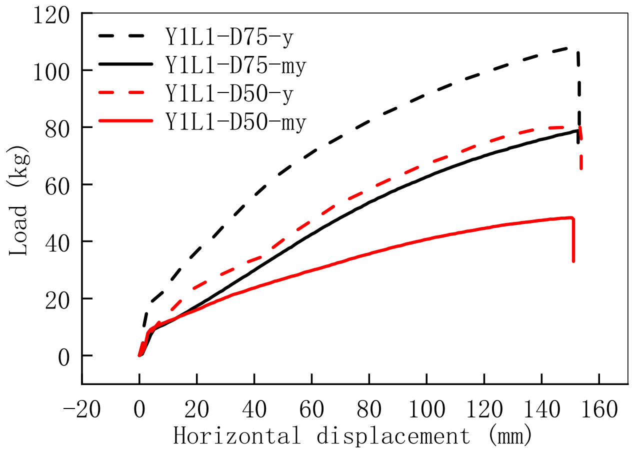

Figure 11. Displacement load curves with different burial depth.

Further analysis is warranted to explore the impact of additional and distributed blades on bearing capacity and its characteristics. In Figure 12, the arrangement of diagrams follows the trend of blade addition: Figure 12a,b reflect the effects of adding blades on the tensile side. Notably, (a) and (b) yield differing results. In (a), the addition of blades has an adverse impact on foundation bearing capacity, while in (b), it has a positive effect. From Figure 12, the disparity in bearing capacity stems from differences in Y-pile configuration. Counterintuitively, a smaller number of blades on the Y-pile results in greater foundation bearing capacity. This trend in shallow burial conditions is contrary to that in deep burial conditions. Taking into account the analysis results in the previous graph, the divergence arises from the load-bearing characteristics of compression and tension piles: in shallow burial conditions, the disparity in bearing capacity between tension and compression piles is more pronounced. When Y-pile blade numbers increase, this disparity only widens, making it harder for compression piles to bear loads and further emphasizing the role of tension piles in determining bearing capacity and failure mode. The outcomes depicted in Figure 12c,d further underline the disadvantage of enhanced compression piles. As shown in Figure 13, a smaller burial depth results in a smaller burial depth of the top blade, because the gap between the bearing capacity of Y1L1-y and Y1L2-y in this study originates from the compressed piles, whereas Figure 12b belongs to the unfulfilled bearing capacity of the compressed piles, which reflects the gap in the ultimate bearing capacity of the tensioned piles.

3.1.2. Single Pile Tensioned Working Condition (d-my)

Building on the preceding analysis, considering the tension load on a single pile in the d-y orientation, the relative bearing capacity between the foundation sides still exhibits variability. On the d-my orientation, where both piles experience compression, the pattern should be straightforward. As supported by Figures 14 and 15, the following observations corroborate earlier analyses: (a) Figure 14a,b depict the reinforcement of tension piles, aligning conspicuously with Figure 15's portrayal (b); (b) Figure 14a,b illustrate the enhancement of compression piles, aligning conspicuously with Figure 12c,d; (c) Figure 15c reveals an amplification in bearing capacity with an increasing number of blade elements in Y-piles. This contradicts Figure 13's trend. Moreover, d-y orientation surpasses d-my when the blade count of Y-piles is one, the difference in bearing capacity between the two loading orientations is most pronounced; (d) Figure 15d illustrates how variations in blade elements affect the relative bearing capacity in different loading orientations. When the blade count of Y-piles is one, the bearing capacity in d-y is approximately 1.6 times that in d-my. As blade count increases to Y2L2, the gap narrows, exhibiting changes in relative size throughout the loading process. Notably, except for the initial phase, the curves for Y2L1 and Y2L2 both show a descending tendency during most of the process, indicating differences in the development of bearing capacity between compression and tension single piles.

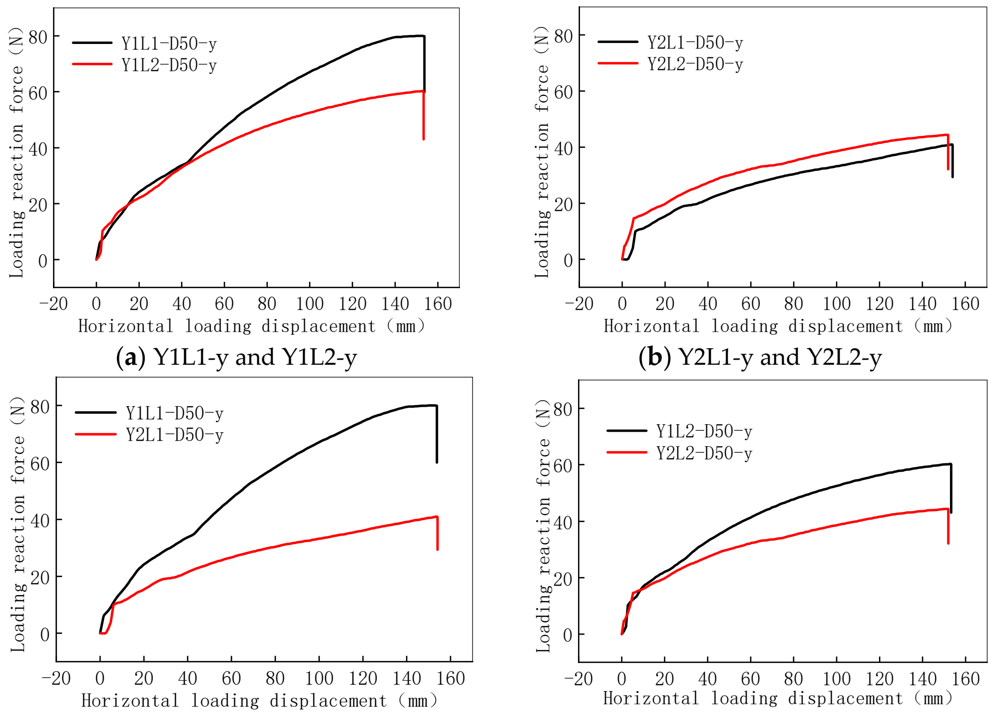

(**a**) Y1L1-y and Y1L2-y (**b**) Y2L1-y and Y2L2-y

(**c**) Y1L1-y and Y2L1-y (**d**) Y1L2-y and Y2L2-y

Figure 12. Displacement load curve of single pile under pressure condition.

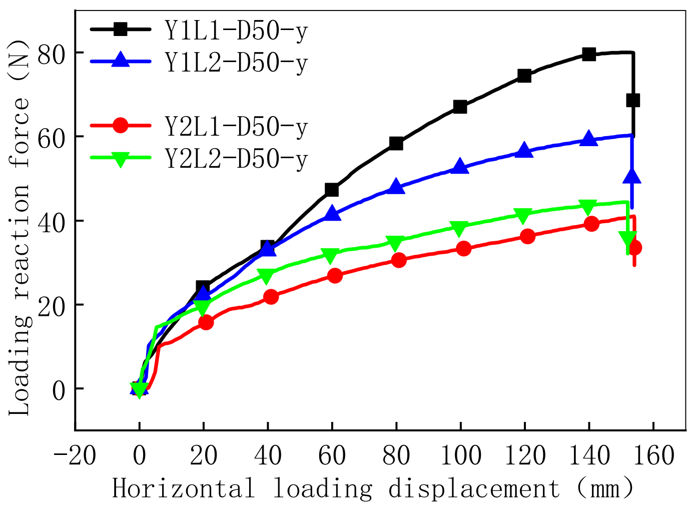

Figure 13. Displacement load curve for each working condition of single pile under pressure.

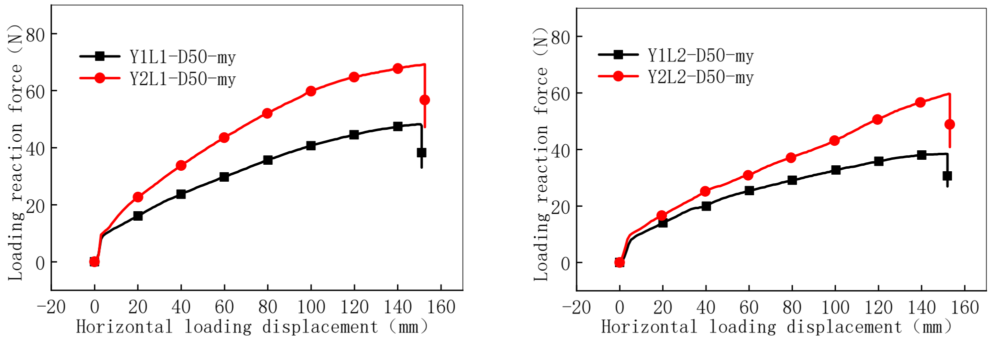

(**a**) Y1L1- my and Y2L1-my (**b**) Y1L2- my and Y2L2-my

Figure 14. Tensile side increase blade displacement (x-mm) load (y-N) curve.

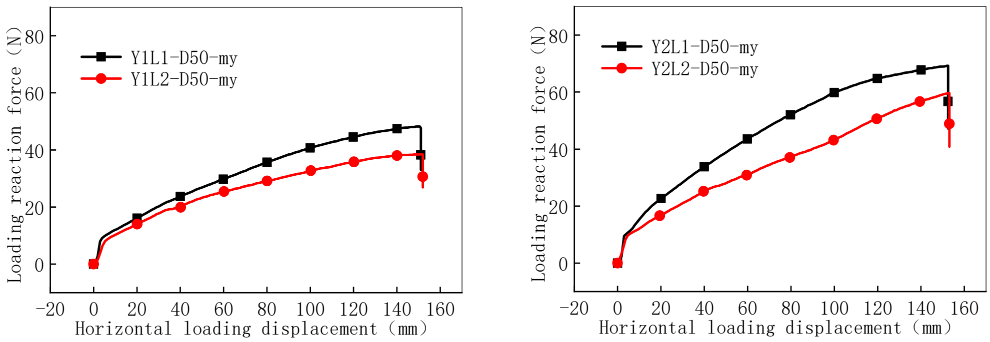

(**a**) Y1L1- my and Y1L2-my (**b**) Y2L1- my and Y2L2-my

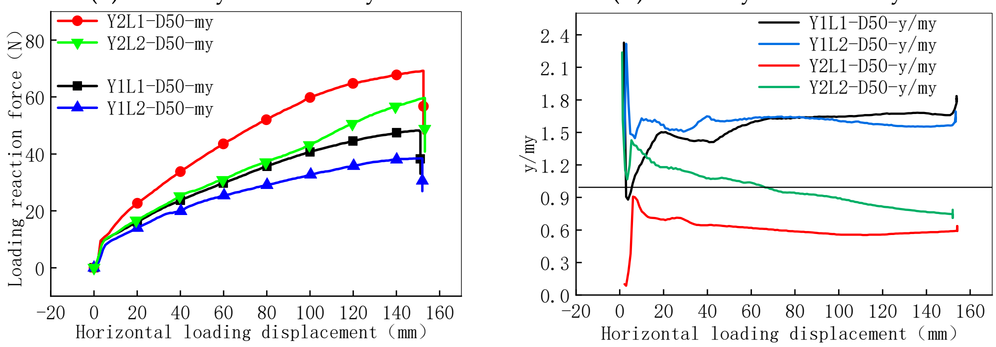

(**c**) Loading reaction force for different working conditions (**d**) Effects of blade increase and decrease for different loading directions

Figure 15. Pressure side increase blade displacement load curve.

3.2. Bearing Mode and Deformation Characteristics of Foundation under Different Burial Depth

3.2.1. Single Pile under Pressure Working Condition (d-y)

Illustrated in Figure 16 is the axial displacement behavior of the foundation with uniform blade distribution. Here, C signifies compression pile and T denotes tension pile. From panel (a), the mode of displacement failure echoes the deep embedding scenario, manifesting as rapid growth in displacement for compression piles, ultimately surpassing tension pile displacement. Yet, comparing the outcomes in panel (b), it is apparent that for Y1L1, the disparity in foundation displacement is more pronounced under relatively shallow embedding. Clearly, the failure of compression piles becomes more evident and direct. The reduction in embedding depth evidently diminishes the bearing capacity of compression piles, consequently reducing the relative magnitude of bearing capacity between the two sides of the foundation. For Figure 17, portraying the case of non-uniform blade distribution, similar displacement failure patterns are observed when compared with deep embedding conditions. Displacement of compression piles is smaller than that of tension piles, and the disparity accentuates in panel (b). This suggests that the increase of a blade element on a compression pile relative to deep embedding amplifies the bearing capacity gap. In shallow embedding, the bearing capacity of both tension and compression piles diminishes considerably due to reduced embedding depth. Consequently, variations in blade elements significantly alter pile bearing capacity and provoke distinct changes in relative magnitude on either side of the foundation.

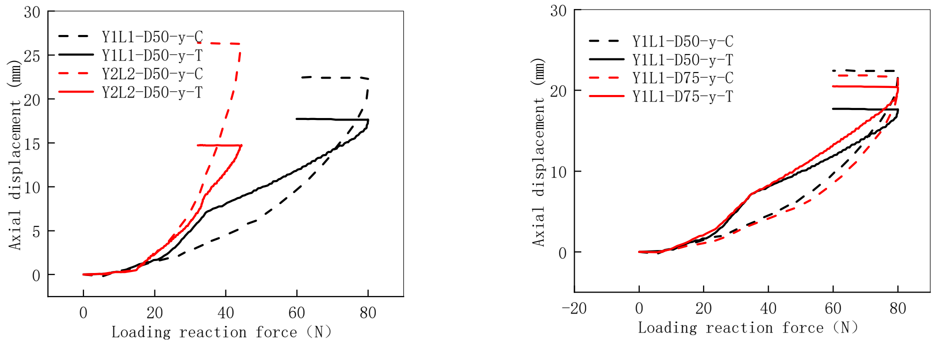

(**a**) Different loading modes (**b**) Different burial depths

Figure 16. Foundation axial displacement with uniform blade distribution.

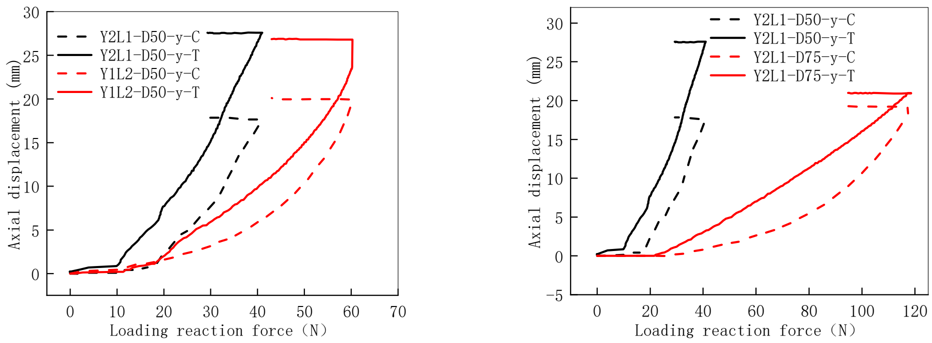

(**a**) Different loading modes (**b**) Different burial depths

Figure 17. Foundation axial displacement in case of uneven blade distribution.

In Figure 18, an understanding of the mutual interaction between the two sides of the foundation is further advanced through an exploration of soil pressure changes at blade locations under compression load. Panel (a) illustrates that increasing blade count for L-piles leads to an augmentation of soil pressure at the bottom of compression piles. Meanwhile, panel (b) demonstrates that reinforcement of compression piles leads to a reduction in soil pressure. Panels (c) and (d) differentiate the soil pressure distribution for Y1L2 and Y2L2 under compression and tension piles, respectively. In panel (c), the soil pressure at the base of compression piles for Y2L2 is less than that for Y1L2, while in panel (d), the initial soil pressure at the upper blade of Y2L2 is higher than Y1L2, signifying a weakening effect on compression piles and an augmented reliance on tension piles.

3.2.2. Single Pile Tensioned Working Condition (d-my)

Figure 19 delves further into the foundation's bearing characteristics in terms of axial displacement. As depicted in (a), when under shallow embedding conditions, the addition of spiral blades on d-my leads to a reduction in displacement for the compression pile and an increase in displacement for the tension pile, thereby widening the gap between them. Similarly, as seen in (b), when compared to deep embedding, both Y1L1 and Y2L2 compression pile displacements diminish, and the disparity between tension and compression pile displacements increases. Both (a) and (b) underscore that under shallow embedding, tension piles exhibit a reduced relative bearing capacity compared to compression piles, accentuating the foundation's shortcoming. As earlier elucidated, mutual interaction and constraint exist between compressed and tension piles in the foundation. The efficacy of the compression pile's bearing capacity hinges on the tensile pile's bearing capacity and restraint, necessitating that the tensile pile possess sufficient load-bearing capacity. However, it is evident that shallow embedding exacerbates the unfavorable situation for the tension loading of individual piles.

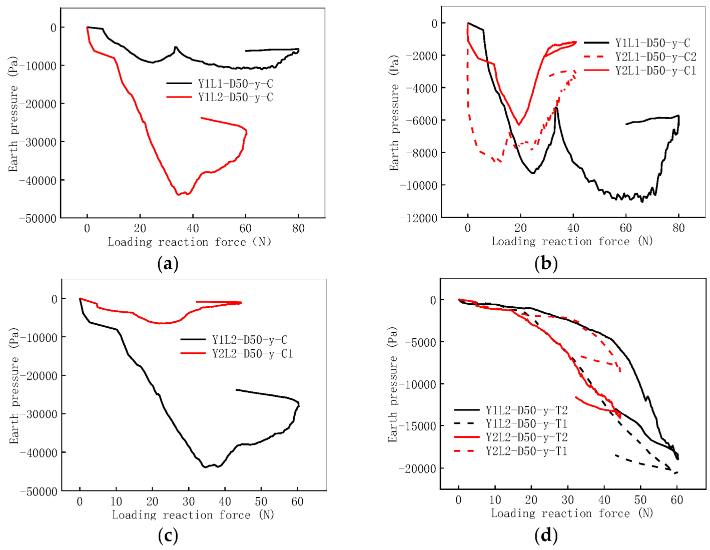

Figure 18. Variation of soil pressure at the blade. (**a**) Y1L1-C and Y1L2-C, (**b**) Y1L1-C, Y2L1-C2 and Y2L1-C1, (**c**) Y1L2-C and Y2L2-C1, (**d**) Y1L1- T2, Y1L2-T1, Y1L2-T1 and Y2L2-C1.

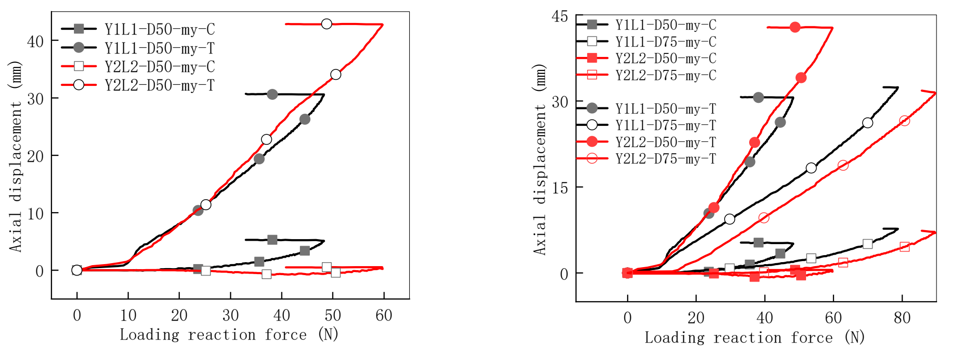

(**a**) Shallow burial conditions (**b**) Comparison of deep and shallow burial

Figure 19. Base axial displacement with uniform blade distribution.

Figure 20 illustrates the displacement state of the foundation with uneven blade distribution. As previously mentioned, the overall displacement trend aligns with the deep embedding scenario, where tension pile displacements surpass those of compression piles. In (a), Y2L1's tension pile displacement is smaller, while the compression pile displacement is greater, rendering a more favorable displacement scenario compared to Y1L2. It is evident that strengthening the compression pile on d-my under shallow embedding proves disadvantageous, as evidenced by the difference in load-displacement curves in Figure 15d. In (b), it is apparent that, compared to deep embedding, shallow embedding results in reduced displacement for compression piles and increased displacement for tension piles, further diminishing the foundation's bearing capacity. This aligns with the aforementioned rationale.

In both (a) and (b) of Figure 21, it is observed that adding blades leads to a decrease in tension pile soil pressure. Although larger tension pile displacements would typically yield higher soil pressures at the blade interface, horizontal displacement should also be considered. To this end, Figure 22 portrays the development of horizontal displacement with applied load at the respective models depicted in Figure 21. Clearly, for the same load, when blades are added to the L pile (compression pile), the horizontal pile displacement increases. This results in greater disturbance to the soil, weakening its strength. Additionally, the increased angle of the pile, influenced by blade interaction with the soil, diminishes the axial impact of the blades, leading to reduced soil pressure and exacerbating the foundation's bearing capacity disparity. The reason for increased horizontal displacement is also evident. The foundation's point of loading necessitates both axial and horizontal displacement, with the former originating from the pile's axial and horizontal movements, and the latter from the pile's top bending. Notably, bending in the pile is negligible in the model experiment. As compression pile axial stiffness increases, horizontal displacement also increases. It is evident that mutual influence and constraint manifest in horizontal displacement as well.

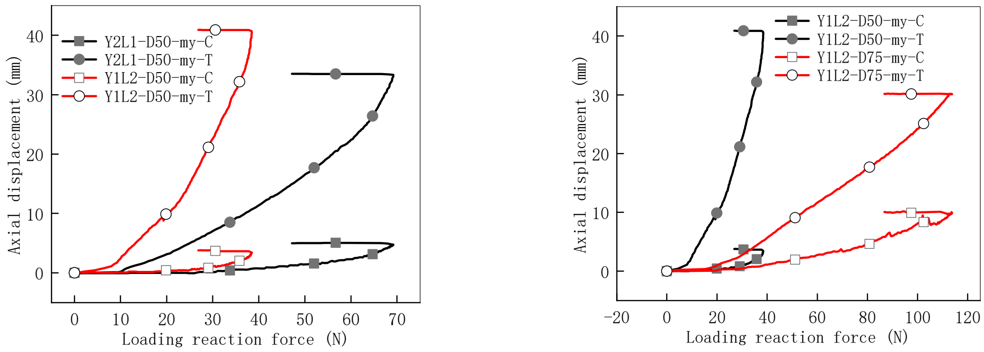

(**a**) Shallow burial conditions (**b**) Comparison of deep and shallow burial

Figure 20. Base axial displacement in case of uneven blade distribution.

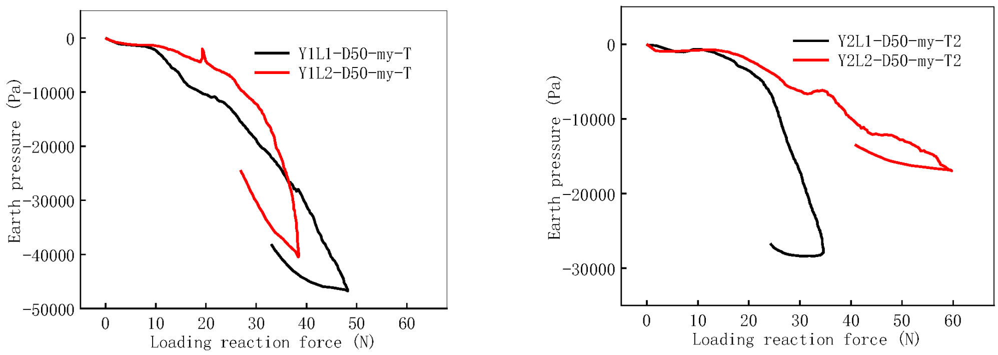

(**a**) Y1L1 and Y1L2 (**b**) Y2L1 and Y2L2

Figure 21. Variation of soil pressure at the blade.

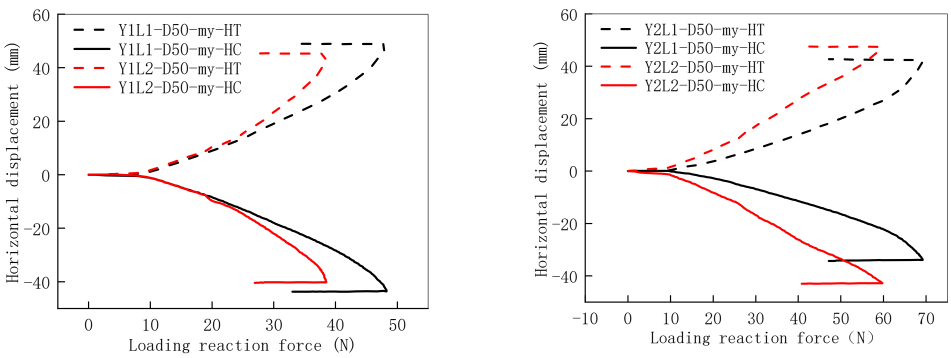

(**a**) Pressurized piles without additional blades (**b**) piles with additional blades

Figure 22. Horizontal displacement of pile foundation.

4. Conclusions

Through the juxtaposition and analytical scrutiny of experimental outcomes under varying embedding depths, this discussion has delved into the foundation's bearing capacity and characteristics across diverse embedding conditions. The salient conclusions are outlined as follows:

(1) The embedding depth wields a profound influence on the foundation's load-bearing capacity. Under the circumstance where the base of the three helix pile guide frame is embedded at 6.5 times the outer diameter of the blade, the bearing capacity far surpasses that of when it is embedded at 4 times the blade diameter. Notably, in the d-my direction, the bearing capacity at 6.5 times the blade diameter approximates twice that of 4 times the blade diameter.

(2) In shallow embeddings, the relative magnitude of load-bearing capacity between tension and compression piles exhibits a wider gap. This leads to an escalation in the disparity between both sides of the foundation with the augmentation of tension piles' blade count. Consequently, it hampers the potential of compression piles' load-bearing capacity, rendering an unfavorable scenario for bearing capacity and failure modes. In essence, in shallow embeddings, the relative compression-side load-bearing capacity diminishes compared to that of deep embeddings, accentuating the foundation's shortcoming in this aspect. The augmentation or reduction of blades yields a considerable impact on pile load-bearing capacity and deformation characteristics. The load-bearing capacity of compression piles is restricted, while tension piles undergo greater displacement, leading to reduced soil pressure on compression piles.

(3) In contrast to deep embeddings, in shallow embeddings, the displacement of compression piles grows at a swifter pace, eventually surpassing that of tension piles. Moreover, the disparity in displacement of compression piles augments with diminishing embedding depth. The impact of blade augmentation on the foundation's load-bearing capacity and deformation characteristics is evident, yet its effectiveness hinges on whether the enhancement occurs on the tension or compression side. Furthermore, the distribution of soil pressure on compression and tension piles exhibits contrasting trends.

In summation, from the analysis of the foundation's load-bearing patterns and deformation characteristics at varying embedding depths, it is apparent that under shallow embedding conditions, the foundation's characteristics and deformation traits are more sensitive to changes in blade configuration. The interplay and mutual restraint between compression and tension piles significantly influence the foundation's load-bearing capacity. Additionally, the increase in horizontal displacement also influences the foundation's load-bearing characteristics. These findings offer crucial reference and guidance for the design and optimization of helical pile guide frame foundations. Further investigation into blade distribution, soil mechanical properties, and the impact of horizontal displacement will provide a comprehensive understanding of the foundation's load-bearing and deformation characteristics, furnishing more precise design criteria for engineering practice.

Author Contributions: Conceptualization, P.Z. and C.O.; methodology, C.O.; software, J.L.; validation, C.O., P.Z., J.L. and T.W.; formal analysis, C.O.; investigation, J.L. and T.W.; resources, C.O.; data curation, P.Z.; writing—original draft preparation, C.O.; writing—review and editing, P.Z.; visualization, J.L. and T.W.; supervision, J.L.; project administration, P.Z.; funding acquisition, C.O. All authors have read and agreed to the published version of the manuscript.

Funding: This research received no external funding.

Conflicts of Interest: The authors have no competing interest to declare that are relevant to the content of this article.

References

1. Bak, H.M.; Halabian, A.M.; Hashemolhosseini, H.; Rowshanzamir, M. Axial response and material efficiency of tapered helical piles. *J. Rock Mech. Geotech. Eng.* **2021**, *13*, 176–187. [CrossRef]
2. Spagnoli, G.; Cavalcanti Tsuha, C.D.H. A review on the behavior of helical piles as a potential offshore foundation system. *Mar. Georesources Geotechnol.* **2020**, *38*, 1013–1036. [CrossRef]
3. Byrne, B.W.; Houlsby, G.T. Helical piles: An innovative foundation design option for offshore wind turbines. *Philos. Trans. R. Soc. a-Math. Phys. Eng. Sci.* **2015**, *373*, 20140081. [CrossRef] [PubMed]
4. Spagnoli, G.; Cavalcanti Tsuha, C.d.H.; Oreste, P.; Solarte, C.M.M. Estimation of Uplift Capacity and Installation Power of Helical Piles in Sand for Offshore Structures. *J. Waterw. Port Coast. Ocean Eng.* **2018**, *144*, 04018019. [CrossRef]
5. Ding, H.; Wang, L.; Zhang, P.; Liang, Y.; Tian, Y.; Qi, X. The Recycling Torque of a Single-Plate Helical Pile for Offshore Wind Turbines in Dense Sand. *Appl. Sci.* **2019**, *9*, 4105. [CrossRef]
6. Emirler, B.; Tolun, M.; Yildiz, A. Investigation on determining uplift capacity and failure mechanism of the pile groups in sand. *Ocean. Eng.* **2020**, *218*, 108145. [CrossRef]
7. Alwalan, M.; Alnuaim, A. Axial Loading Effect on the Behavior of Large Helical Pile Groups in Sandy Soil. *Arab. J. Sci. Eng.* **2022**, *47*, 5017–5031. [CrossRef]
8. Liu, Z.; Kong, G.; Wen, L.; Wang, Z.H. Model tests on uplift and lateral bearing characteristics of inclined helical pile group embedded in sand. *Rock Soil Mech.* **2021**, *42*, 1944–1950.
9. Dong, T.; Zhang, Y.; Li, S.; Huang, L. Bearing capacity of screw pile group determined by inclined pull-out test. *Chin. J. Geotech. Eng.* **2008**, *30*, 429–433.
10. Dong, T.; Liang, L. Solution of load-settlement function of single screw pile under axial pressure. *Chin. J. Geotech. Eng.* **2007**, *29*, 1483–1487.
11. George, B.E.; Banerjee, S.; Gandhi, S.R. Numerical analysis of helical piles in cohesionless soil. *Int. J. Geotech. Eng.* **2020**, *14*, 361–375. [CrossRef]
12. Vignesh, V.; Muthukumar, M. Experimental and numerical study of group effect on the behavior of helical piles in soft clays under uplift and lateral loading. *Ocean. Eng.* **2023**, *268*, 113500. [CrossRef]
13. Chong, G. Optimization of offshore wind power multi pile jacket foundation jacket. *Technol. Style* **2017**, 128–129+147. [CrossRef]
14. Zhou, K.; Zhang, X.; Zeng, Q. Discussion design of multiple jacket for offshore wind turbines. *Shanxi Archit.* **2015**, *41*, 65–67.
15. Livneh, B.; Naggar, M.E. Axial testing and numerical modeling of square shaft helical piles under compressive and tensile loading. *Can. Geotech. J.* **2008**, *45*, 1142–1155. [CrossRef]
16. Clemence, S.P. Uplift behavior of anchor foundations in soil. In Proceedings of the Session Sponsored by the Geotechnical Engineering Division of the American Society of Civil Engineers in Conjunction with the ASCE Convention, Detroit, MI, USA, 24 October 1985.
17. Mitsch, M.P.; Clemence, S.P. The uplift capacity of helix anchors in sand. In *Uplift Behavior of Anchor Foundations in Soil*; American Society of Civil Engineers: Reston, VA, USA, 1985.
18. Mooney, J.S.; Adamczak, S.; Clemence, S.P. Uplift Capacity of Helical Anchors in Clay and Silt. In *Uplift Behavior of Anchor Foundations in Soil*; American Society of Civil Engineers: Reston, VA, USA, 1985.
19. Mukherjee, S.; Kumar, L.; Choudhary, A.K.; Babu, G.S. Pullout resistance of inclined anchors embedded in geogrid reinforced sand. *Geotext. Geomembr.* **2021**, *49*, 1368–1379. [CrossRef]
20. Rao, S.N.; Prasad, Y.V.S.N. Estimation of uplift capacity of helical anchors in clays. *Geotech. Eng.* **1993**, *119*, 352–357. [CrossRef]
21. Abdrabbo, F.M.; El Wakil, A.Z. Laterally loaded helical piles in sand. *Alex. Eng. J.* **2016**, *55*, 3239–3245. [CrossRef]
22. Spagnoli, G. Some considerations regarding the use of helical piles as foundation for offshore structures. *Soil Mech. Found. Eng.* **2013**, *50*, 102–110. [CrossRef]